MTF AND POINT-SPREAD FUNCTION FOR A LARGE-AREA CCD IMAGER*

K. J. Ando
Jet Propulsion Laboratory
Pasadena, California

In the present work, utilizing the Crowell and Labuda model, the MTF degradation due to lateral diffusion is calculated for a back-illuminated CCD imager for typical device parameters. The discrete nature of the CCD and finite size of the photosensitive elements, with its less than ideal collection efficiency for photogenerated charge, result in an additional MTF degradation. The Fourier transform approach is utilized to calculate the effective point-spread function for these processes in the time domain. Experimental data is presented on the point-spread function for a three-phase, double-level anodized aluminum 160 X 100 thinned and back-illuminated CCD imager and compared with the theoretical results. A simple modification of the Crowell and Labuda model suggested by these results is presented. Finally, the effects of the less than ideal charge transfer efficiency in practical devices are calculated and applied to predict the anticipated MTF and point-spread function for a 400 X 400 large-area CCD imager currently under development.

I. INTRODUCTION

The charge-coupled device offers a new and significant approach to achieving the once elusive goal of a viable large-area solid-state imager

*This paper presents the results of one phase of research carried out at the Jet Propulsion Laboratory, California Institute of Technology, under Contract No. NAS 7-100, sponsored by the National Aeronautics and Space Administration.

possessing the format size and element density comparable to a conventional vidicon. Considerable progress has been made towards achieving this goal, as reflected by the performance data presented at this Symposium on large-area array imagers. This paper discusses the MTF, point-spread function, and the effects of charge transfer inefficiency for such large-area arrays. Expressions for the MTF and point-spread function are derived and applied to a thinned, back-illuminated 400 X 400 area imager (Ref. 1). The results indicate the anticipated performance levels for such a CCD and the significant role of charge transfer efficiency for large-area arrays.

II. MTF AND POINT-SPREAD FUNCTION FOR LATERAL DIFFUSION

Figure 1 illustrates the simplified model utilized by Crowell and Labuda (Ref. 2) to calculate the quantum efficiency η_0 and the MTF for a silicon diode array target. The depletion region of width $L_b - L_a$ is assumed to be totally depleted and a region of zero lateral conductivity. η_0 and the MTF are calculated by evaluating, for a sinusoidal optical input, the steady-state diffusion current

$$J_p = -D\frac{\partial p}{\partial x}\Big|_{y = L_a} \tag{1}$$

flowing into the depletion region from the field-free region and adding the photogenerated current from the direct photon absorption in the depletion region. J_p is evaluated from the solution of the continuity equation

$$-D\nabla^2 p + \frac{p}{\tau} = G(x, y, z) \tag{2}$$

subject to the boundary conditions

$$\begin{aligned} Sp &= \frac{\partial p}{\partial x}\Big|_{y = 0} \qquad \text{(input surface)} \\ p &= 0\Big|_{y = L_a} \qquad \text{(depletion region edge)} \end{aligned} \tag{3}$$

where

p = minority carrier density in excess of thermal equilibrium

τ = minority carrier lifetime

D = minority carrier diffusion constant (cm^2/sec)

$G(x, y, z)$ = minority carrier generation rate per unit volume

S = surface recombination velocity (cm/sec)

The photogeneration rate $G(x, y, z)$ is assumed to vary sinusoidally in the transverse direction and exponentially in the y direction, and is given by

$$G(x, y, z) = \frac{N_0}{2}(1 - R)\alpha \exp(-\alpha y)(1 + \cos kx) \tag{4}$$

where

N_0 = peak incident photon flux

α = silicon absorption coefficient at the wavelength of interest

R = reflectivity of silicon at the wavelength of interest

$k = 2\pi/\lambda$ = spatial frequency of the optical input

The resulting solution can be written in the form

$$J_p(x) = \frac{N_0}{2}(\eta_0 + \eta_k \cos kx)$$

with

$$\eta_k = \frac{\alpha L(1 - R)}{\alpha^2 L^2 - 1}\left[\frac{2(\alpha L + SL/D) - (\beta_+ - \beta_-)\exp(-\alpha L_a)}{\beta_+ + \beta_-} - \frac{1}{\alpha L}\exp(-\alpha L_a)\right]$$

$$-(1-R)\exp(-\alpha L_b) \tag{5}$$

and

$$\eta_0 = \eta_{k=0}$$

where

$$\beta_{\pm} = \left(1 \pm \frac{SL}{D}\right) \exp \pm \frac{L_a}{L}$$

$$L_0 = \text{diffusion length} = (D\tau)^{1/2}$$

$$L = \frac{L_0}{\left(1 + k^2 L_0^2\right)^{1/2}}$$

The MTF, defined to be the peak-to-peak minority carrier current entering the continuous p region normalized with respect to the response for uniform light, is simply the ratio η_k/η_0. The resulting MTF can be written as a sum of a frequency-dependent component and a constant,

$$\frac{\eta_k}{\eta_0} = \frac{\eta(\omega)}{\eta_0} + \frac{C}{\eta_0} \tag{6}$$

where

$$C = \exp(-\alpha L_a)\left\{1 - \exp\left[-\alpha(L_b - L_a)\right]\right\}$$

$\eta(\omega)/\eta_0$ is the output modulation due to absorption in the field-free region and decreases due to lateral diffusion as the input spatial frequency is increased. C/η_0, on the other hand, is equal to the fraction of the total collected charge contributed by direct photon absorption in the depletion region and contributes a constant output modulation. This latter term arises from the total depletion approximation.

The above results can also be applied to a thinned, back-illuminated CCD imager such as that shown schematically in Figure 2. For a typical oxide thickness, clock voltages, and substrate resistivity, the maximum depletion depth is

approximately 5 μm. The depletion depth x_d, however, is not constant throughout the unit cell but varies schematically, as illustrated in Figure 2. Typically, for a three-phase CCD, only approximately 1/3 of the unit cell is depleted to the maximum depth, with the remainder of the unit cell being only partially depleted. The exact profile can be obtained from the surface potential profile $\varphi_s(x)$, since

$$x_d = \left(\frac{2\epsilon\varphi_s(x)}{qN_a}\right)^{1/2} \tag{7}$$

where ϵ is the dielectric constant of silicon and N_a is the acceptor density of the substrate. Additionally, $\varphi_s(x)$ is, in general, anisotropic, with the doping and width of the channel stops being important factors in the direction perpendicular to the channel stops. However, the quantum efficiency is relatively insensitive to the detailed shape of the potential wells. Although partial depletion introduces a transition region of charge collection uncertainty and cross modulation between the unit cells, the total collection efficiency remains unity since the recombination loss is small in this region.

Finally, at wavelengths greater than 0.8 μm, one can expect interference effects due to multiple reflections from the structured side of the CCD. Seib (Ref. 3) has extended the Crowell and Labuda model to include the effects of multiple reflections for normal incidence. His results show that for wavelengths greater than 0.8 μm, although the calculated η_0 is increased over the single pass case, the resulting MTFs are nearly identical. Thus, although the total depletion condition is not realized in practice by a back-illuminated CCD, and multiple reflections are not considered at the longer wavelengths, one nevertheless should obtain a reasonable estimate of the quantum efficiency η_0 and the MTF degradation due to lateral diffusion from the single-pass Crowell and Labuda model. Equation (6) has been evaluated utilizing typical CCD parameters for two substrate thicknesses, and the results are shown in Figures 3 and 4. For a thinned array, the results are relatively insensitive to the value of L_0 and to S. The key parameter, especially at short wavelengths, is the thickness of the field-free region. MTF (∞) is the constant to which the curves converge and is equal to C/η_0.

The results can also be expressed in the time domain by calculating the inverse Fourier transform of Equation (6) to yield the point-spread function for lateral diffusion,

$$PSF(x) = \mathcal{F}^{-1}\left\{\frac{\eta_k}{\eta_0}\right\} = \frac{1}{2\pi}\int_{-\infty}^{\infty}\frac{\eta(\omega)}{\eta_0}\exp(-i\omega x)d\omega + \frac{C}{\eta_0}\delta(x) \qquad (8)$$

Since the lateral diffusion process possesses even symmetry, it is only necessary to evaluate the real part of the complex Fourier transform. Equation (8) was evaluated by numerical integration. The results are shown in Figures 5 and 6 and represent the spatial charge spread (impulse response) of the field-free region to a delta optical input.

III. EFFECTS OF SAMPLING AND THE FINITE PIXEL SIZE

In addition to the MTF degradation resulting from lateral diffusion, the discrete and finite aperture of a CCD imager imposes a further geometric limitation on the MTF. The resulting MTF loss can be estimated by assuming total depletion and dividing the depletion region into contiguous pixels of width d, where d is the pitch of the pixels, as shown in Figure 2. Under these simplifying assumptions, the MTF for the sampling and collection process is given by

$$R_P = \text{sinc}\frac{kd}{2} \qquad (9)$$

The total pixel MTF becomes $\eta_k/\eta_0 \times R_P$ and is plotted in Figure 7 for a typical pixel size of 1 mil. Note that in the spatial frequency range of interest ($f < f_{NYQ}$), the pixel size is the dominant factor. Additionally, the spectral dispersion in the MTF curves has been reduced. The corresponding point-spread function has been calculated by first truncating the MTF expression to zero at f = 4000 c/mm and numerically integrating up to this limit. The results are shown in Figure 8. The error introduced by truncation is negligible for λ = 0.4 and 0.6 μm, whereas for λ = 0.8 μm, the actual point-spread function should be slightly more rectangular than calculated.

The response of a single pixel is given by

$$R(x) = K\int_{-\infty}^{\infty} I(x')PSF(x' - x)dx' \qquad (10)$$

where I(x') is the spread function for the optical input. If I(x') is narrow in comparison with PSF(x), it follows from the sifting properties of the delta function that

$$R(x) \cong PSF(x) \qquad (11)$$

Thus, by measuring the response of a single pixel as a point or narrow slit light source is scanned across the pixel, the point-spread function of the device can be experimentally determined. The next section will describe the results of such a measurement on a thinned, back-illuminated CCD imager.

IV. EXPERIMENTAL RESULTS

The characteristics of the tested CCD and the operating conditions for these measurements, respectively, are summarized below. Design and general performance data has been presented previously on this type of CCD imager (Ref. 4).

(1) CCD imager characteristics

- (a) Three-phase, double-level anodized aluminum
- (b) Surface channel
- (c) Thinned and back-illuminated
- (d) Array size - 160 pixels horizontal by 100 pixels vertical (160 × 120 mils)
- (e) Pixel size - 1.0 × 1.2 mils

(2) Operating conditions for pixel sensitivity profile measurements

- (a) Serial clock frequency = 100 kHz
- (b) Serial fat zero ≈ 10%

(c) Exposure time = 250 msec (shuttered)

(d) Total frame time = 423 msec

The point-spread function measurements were made with the apparatus shown in Figure 9. The point light source was a 5-mil Xenon arc lamp, which was imaged through a 10 × F/2 microscope objective. The CCD was approximately 200 cm from the light source. Spectral and neutral density filters were inserted into the optical path to vary the spectral passband and intensity of the light spot. The light spot could be viewed simultaneously through a microscope eyepiece via a beam splitter as it was being focused on the CCD input surface. The diameter of the minified light spot, as visually determined by focusing the light spot onto a stage micrometer placed in the same plane as the CCD input surface, was less than 4 μm. The light spot was stepped across the CCD in the parallel transfer section in 2.2-μm increments in the image plane. The output from a 20 × 20 area (400 pixels) was recorded after a 12-bit A/D conversion by a digital tape recorder after each 2.2-μm increment. The data was taken from a computer printout of the 20 × 20 area. Figure 10 shows the typical video output as the spot was scanned across three adjacent pixels. The assymetric response is due to the redistribution of a fraction of the charge from the primary pixel into the trailing pixels because of charge transfer inefficiency.

Typical results showing the simultaneous output from three adjacent pixels as a function of spot position are shown in Figures 11 and 12, respectively. A Beck glass filter with a long-wavelength cutoff of 0.45 μm was utilized. The spot intensity was adjusted to be approximately one-half of full well. The spot was positioned as close as possible to the output to minimize charge transfer efficiency effects. The peak amplitude increased from pixel to pixel because of the localized shading in the region near the output. The slight assymetry in the measured profiles is due to charge transfer inefficiency. The solid lines enclosing the sensitivity profiles are the boundaries of the respective pixel. Similar measurements were also made with a Beck red glass filter, and essentially identical results were obtained.

Comparison of the sensitivity profiles with the calculated point-spread functions of Figure 8 shows that the measured profile is narrower at the center and exhibits more response outside the pixel than predicted by the Crowell and

Labuda model, indicating some pixel overlap. A simple modification of this model is suggested by these results, as shown in Figure 13. The collection regions defining the pixels are assumed to be overlapping and trapezoidal in shape to account for the less than ideal isolation between pixels. The total collection efficiency for the depletion region remains unchanged since the sum of the collection efficiencies in the overlap region is unity. Because of this overlap, the MTF due to the collection process is reduced from R_P to R_T, where

$$R_T = \text{sinc}\frac{\omega b}{2}\,\text{sinc}\frac{\omega(a+b)}{2} \tag{12}$$

V. CHARGE TRANSFER INEFFICIENCY EFFECTS ON A LARGE-AREA ARRAY

In an image sensor such as a vidicon, the electron beam provides a direct readout of each pixel. On the other hand, in a CCD, the signal charge from each pixel must first be transferred to the output for readout. In practical devices, the transfer process is less than perfect, with some charge redistribution and loss occurring in the transfers and the dispersion increasing with the number of transfers. The key characteristic of a CCD is its charge transfer efficiency. The frequency-dependent distortion introduced by charge transfer inefficiency for a CCD delay line for the case where the fixed loss is negligible has been calculated utilizing both Z transform (Refs. 5 and 6) and Fourier analysis (Refs. 7, 8, and 9). The transfer function, derived from the transform of the impulse response in the time domain, for such a delay line is given by (Refs. 5 and 7)

$$H(\omega) = A(\omega)\exp\left[-i\varphi(\omega)\right] \tag{13}$$

where

$$\left|A(\omega)\right| = \left[\frac{(1-\epsilon)^2}{1+\epsilon^2-2\epsilon\cos\omega d}\right]^{n/2}$$

and

$$\varphi(\omega) = n \tan^{-1} \frac{\epsilon \sin \omega d}{1 - \epsilon \cos \omega d}$$

where ϵ is the fraction of charge left behind per transfer, n is the number of transfers, and d is the pitch of the pixels. The modulus $A(\omega)$ is the attenuation factor, and the argument $\varphi(\omega)$ is the phase shift. For $\epsilon << 1$, these expressions can be approximated by (Refs. 7 and 10)

$$\begin{aligned} \left|A(\omega)\right| &\cong \exp(-n\epsilon)(1 - \cos \omega d) \\ \varphi(\omega) &\cong n\epsilon(\omega d - \sin \omega d) \end{aligned} \tag{14}$$

In the time domain, which is the more suitable domain to calculate pulse train dispersion effects, the charge $Q_N(nt_0)$ in a charge packet at a time nt_0, transferred through N pixels, is given by (Ref. 11)

$$Q_N(nt_0) = (1 - \epsilon)^N Q_0[(n - N)t_0] + Q_R(nt_0) \tag{15}$$

where

$$Q_R(nt_0) = (1 - \epsilon)^N \sum_{m=1}^{\infty} \binom{N+m}{m} \epsilon^m Q_0[(n - N - m)t_0]$$

Here t_0 is the clock period, $Q_0(nt_0)$ is the size of the charge packet inserted at the input at time nt_0, and Q_R is the contribution from the trailers from the preceding charge packets.

Utilizing Equations (14) and (15), the effects of charge transfer inefficiency on the MTF and point-spread function for a large-area CCD imager can be calculated. The results are shown in Figures 14 and 15. Figure 14 is the calculated MTF for a 400 × 400 three-phase CCD imager with a 0.9 × 0.9 mil pixel size

currently under development (Ref. 1) for three locations in the image plane. Overlapping pixels with trapezoidal collection profiles are assumed as shown. Charge transfer efficiencies in the anticipated range for a buried-channel device were used. For $f \ll f_{NYQ}$, the output modulation for a sine-wave input will be identical to the MTF. For optical inputs near f_{NYQ}, however, phasing effects become significant and the output modulation will depend upon the phasing (Δx) between the optical input and the CCD, as shown in Figure 16, where the relations between the MTF and device response for sine- and square-wave inputs have been summarized (Ref. 12).

Figure 15 is the corresponding charge dispersion at the same locations for various optical inputs. The first column shows the effects of charge transfer inefficiency on a single 1, which would roughly be the point-spread function for this array. For a single 1, the ratio of the first trailer to the primary charge packet is equal to $n\epsilon$. Column 2 indicates the output modulation at the Nyquist limit for the in-phase condition. Figures 14 and 15 indicate how the MTF and point-spread function can be expected to vary continuously across the image plane and represents the ideal case, where the charge transfer loss is uniformly distributed. In practical large-area devices, however, charge dispersion will usually occur because of the presence of isolated regions of poor charge transfer efficiency. For such a case, the results shown in Figures 14 and 15 can still be applied by determining an effective $n\epsilon$ product for the region in question.

VI. CONCLUSIONS

The MTF and point-spread function for a large-area CCD imager have been calculated. Both the theoretical model and the experimental results show that the MTF loss due to lateral diffusion in the frequency range of interest ($f < f_{NYQ}$) is minimal for a back-illuminated CCD thinned to 10 μm, with the size of the pixel and its geometric collection profile being the dominant factor. These results suggest that the MTF could be increased by a further reduction in device geometry before diffusion effects become significant. The key role of charge transfer efficiency has been shown. A charge transfer efficiency η of 0.9999/transfer or better will be necessary to minimize charge dispersion effects and obtain a device where the MTF and point-spread function are limited only by pixel size.

ACKNOWLEDGEMENTS

The author wishes to thank C. J. Mahoney and G. R. Root for their assistance in the experimental phase of this work.

REFERENCES

1. G. A. Antcliffe, L. J. Hornbeck, J. M. Younse, J. B. Barton, and D. R. Collins, Proceedings of this Symposium.
2. M. H. Crowell and E. F. Labuda, Bell Systems Tech. J, 48, 1481 (1969).
3. D. H. Seib, IEEE Tran. Elec. Devices, ED-21, 210 (1974).
4. G. A. Hartsell and A. R. Kmetz, IEDM Tech. Digest, 1974 International Electron Devices Meeting, Washington, D.C., p. 59 (1974).
5. G. F. Vandstone, J. B. G. Roberts, and A. E. Long, Solid State Electronics, 17, 889 (1974).
6. D. D. Buss, W. H. Bailey, and D. R. Collins, Proc. IEEE Int. Symp. Circuit Theory, April 3-7, 1973, pp 3-7.
7. R. D. Nelson and W. P. Waters, Proceedings of the CCD Applications Conference, San Diego, Sept. 18-20, 1973, p. 207 (1973).
8. W. B. Joyce and W. J. Bertram, Bell Systems Tech. J., 50, 1741 (1971).
9. K. K. Thornber, Bell Systems Tech. J., 52, 1453 (1973).
10. M. F. Tompsett, J. Vac. Sci. Technol., 9, 1166 (1972).
11. K. K. Thornber, IEEE J. Solid-State Circuits, SC6, 285 (1974).
12. J. W. Coltman, J. Optical Soc. Am., 44, 468 (1954).

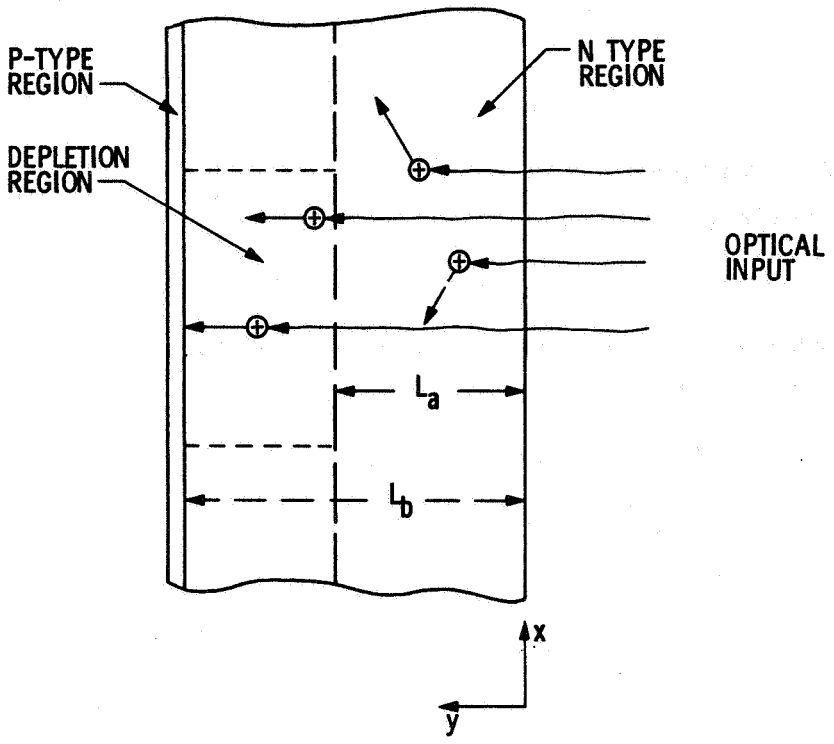

Figure 1. Schematic of simplified model used to calculate η_0 and MTF of a diode array target

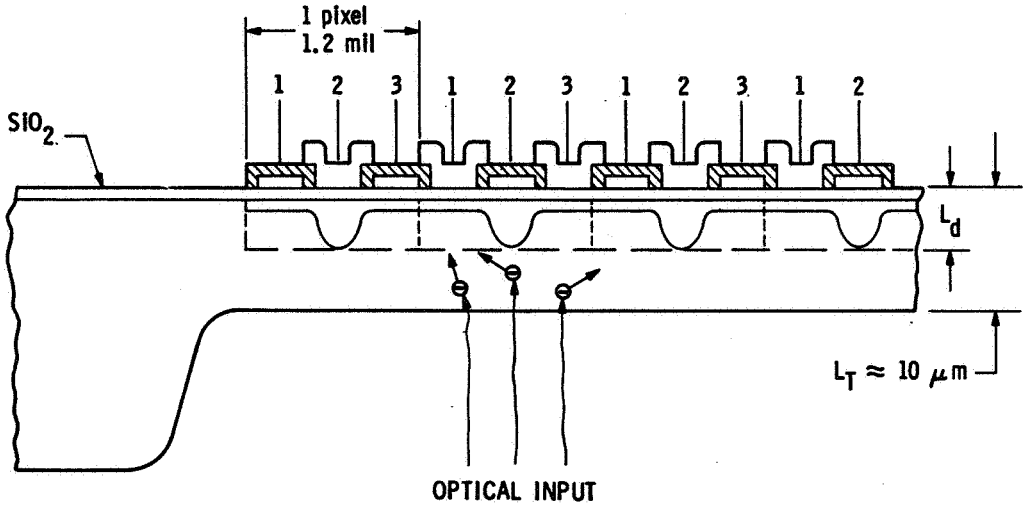

Figure 2. Thinned three-phase anodized AℓCCD (cross section along vertical channel)

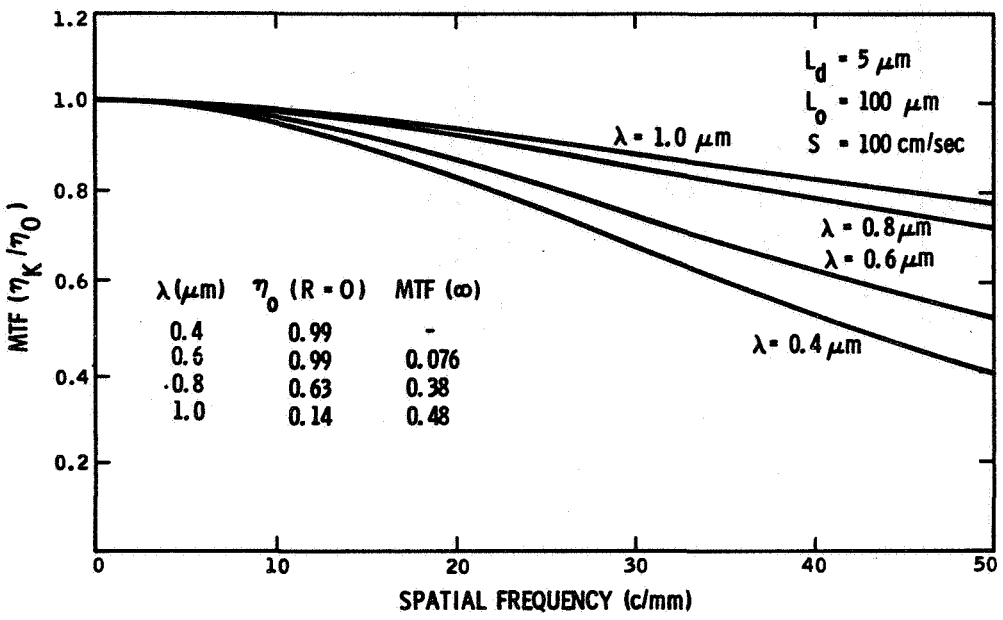

Figure 3. MTF for lateral diffusion (L_T = 10 μm)

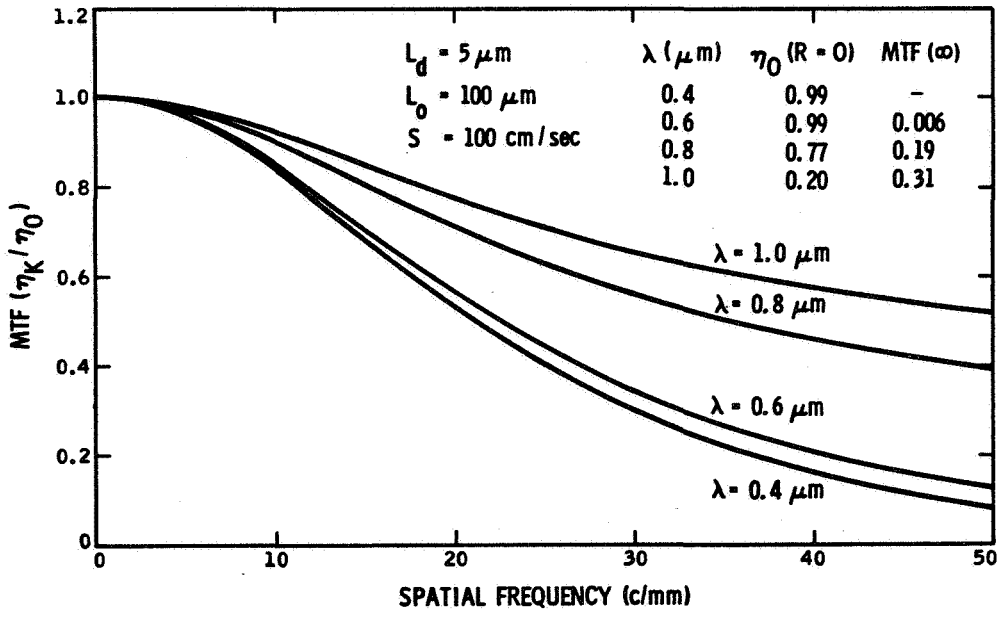

Figure 4. MTF for lateral diffusion (L_T = 15 μm)

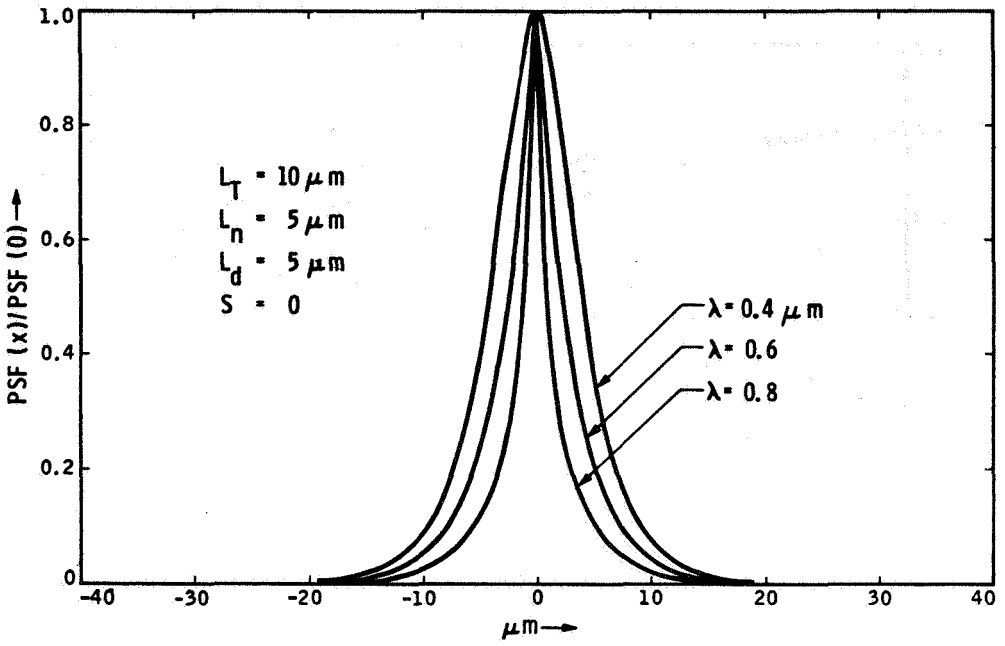

Figure 5. Point-spread function for lateral diffusion $\mathcal{F}^{-1}(\eta_k/\eta_0)C = 0$ (L_T = 10 μm)

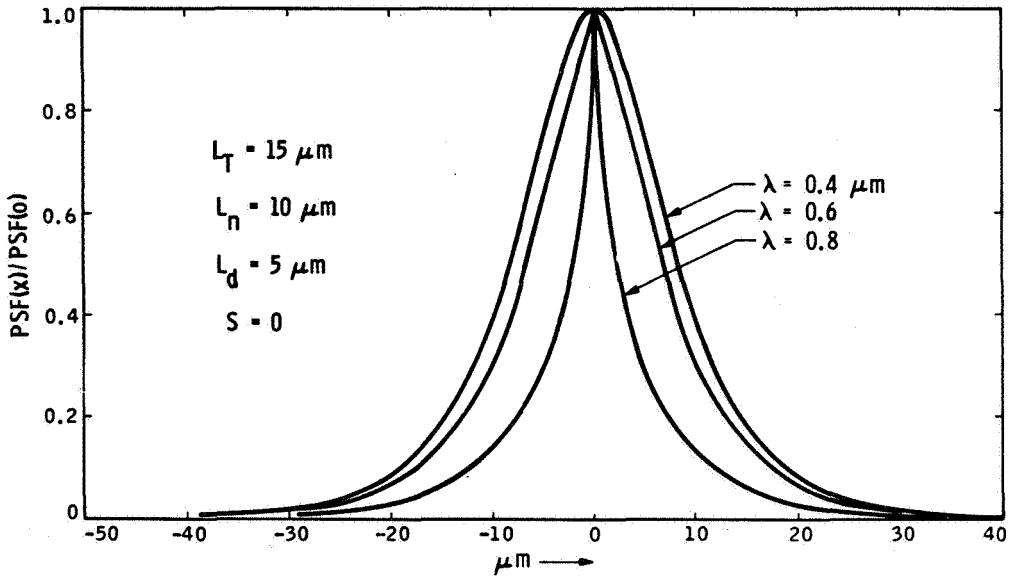

Figure 6. Point-spread function for lateral diffusion $\mathcal{F}^{-1}(\eta_k/\eta_0)C = 0$ (L_T = 15 μm)

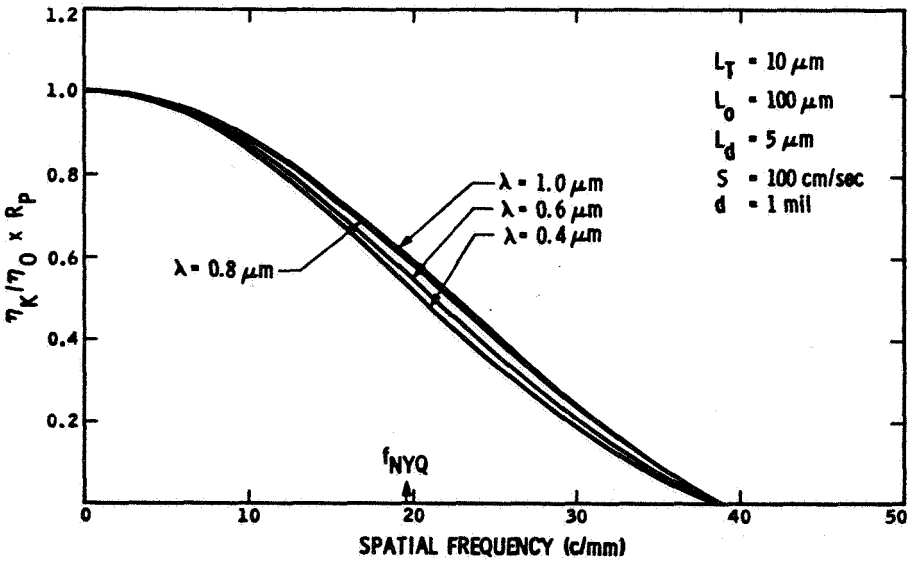

Figure 7. MTF, including the effect of finite pixel size

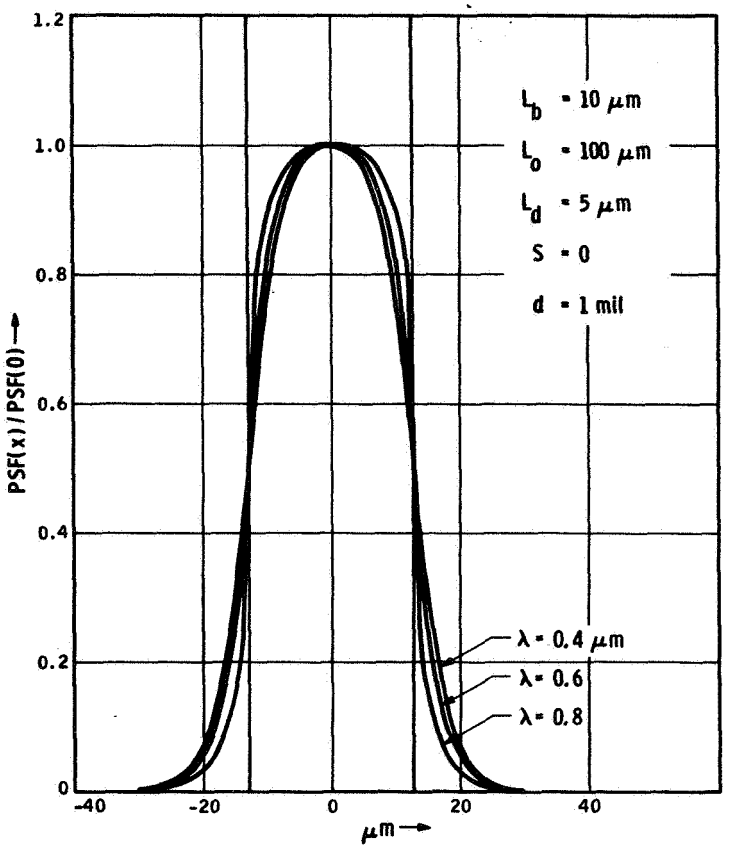

Figure 8. Point-spread function $\mathcal{F}^{-1}(\eta_k/\eta_0 \times R_P)$

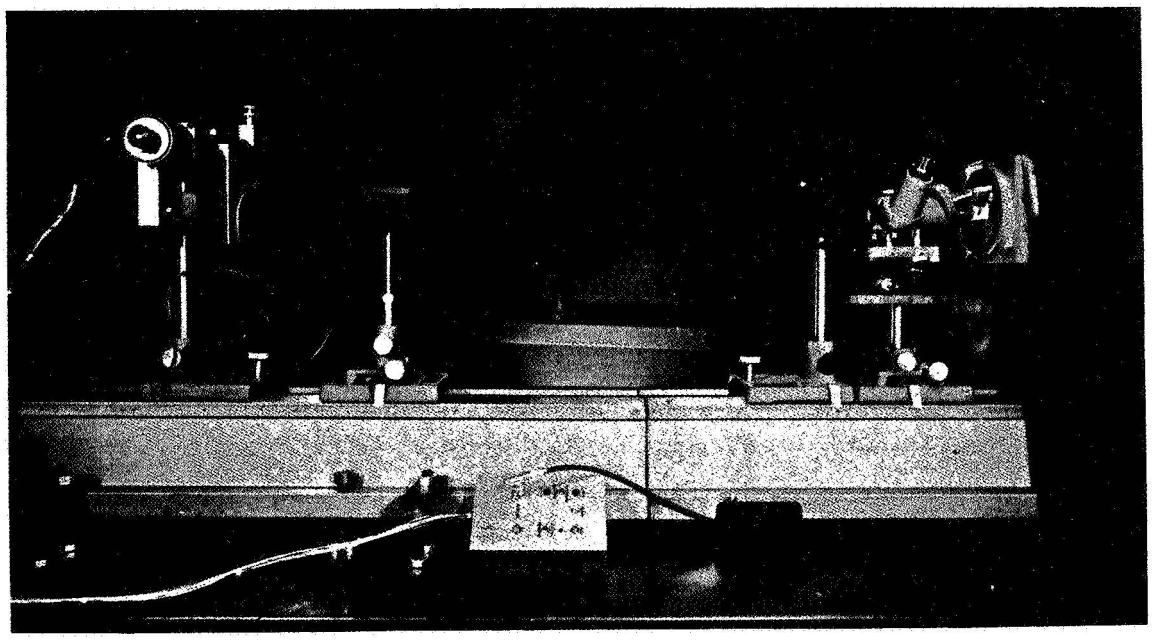

Figure 9. Test setup for sensitivity profile measurements

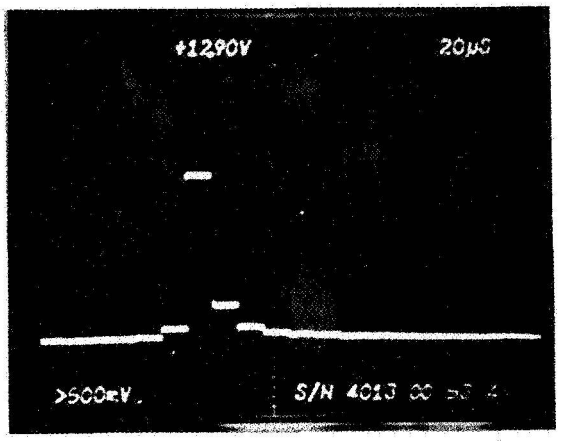

SPOT CENTERED ON PIXEL (25, 7)

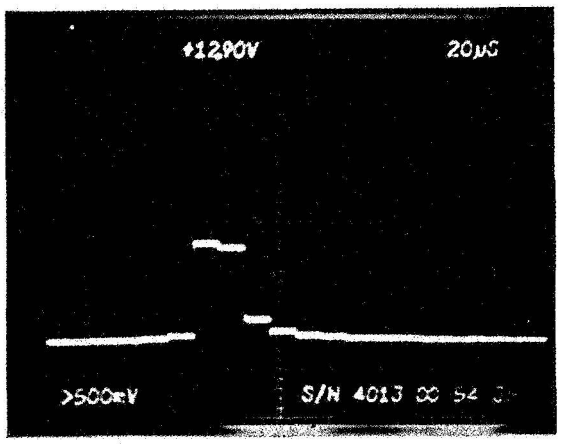

SPOT CENTERED BETWEEN PIXELS (25, 7) AND (26, 7)

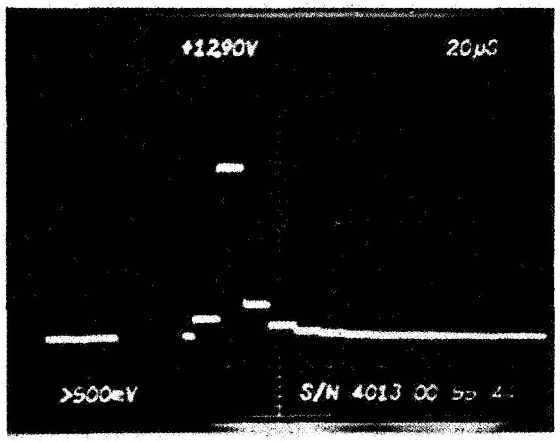

SPOT CENTERED ON PIXEL (26, 7)

Figure 10. Video output from three adjacent pixels vs. spot position (horizontal scan)

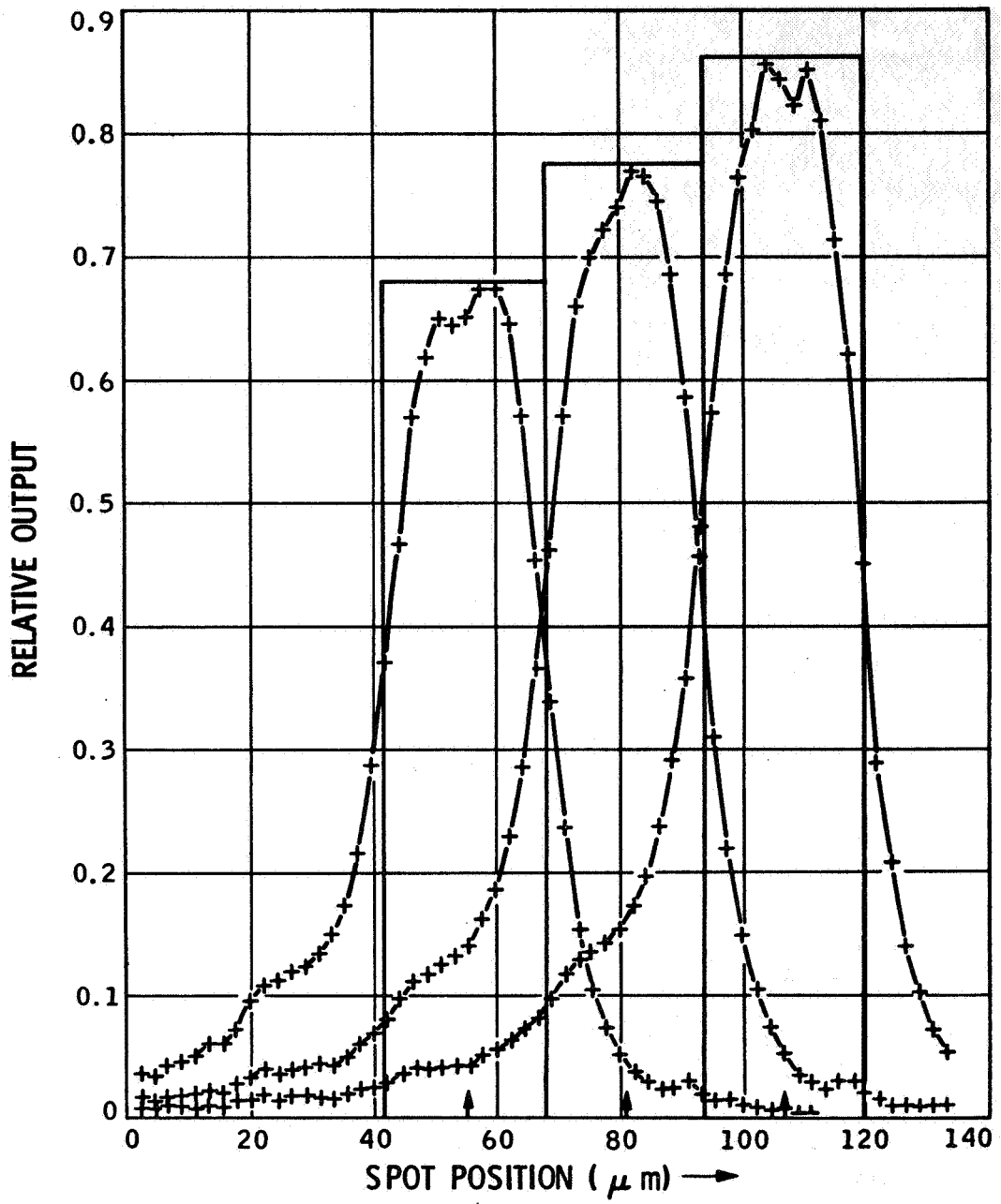

Figure 11. Sensitivity profile for three adjacent pixels (blue filter) (scan ⊥ to vertical channel)

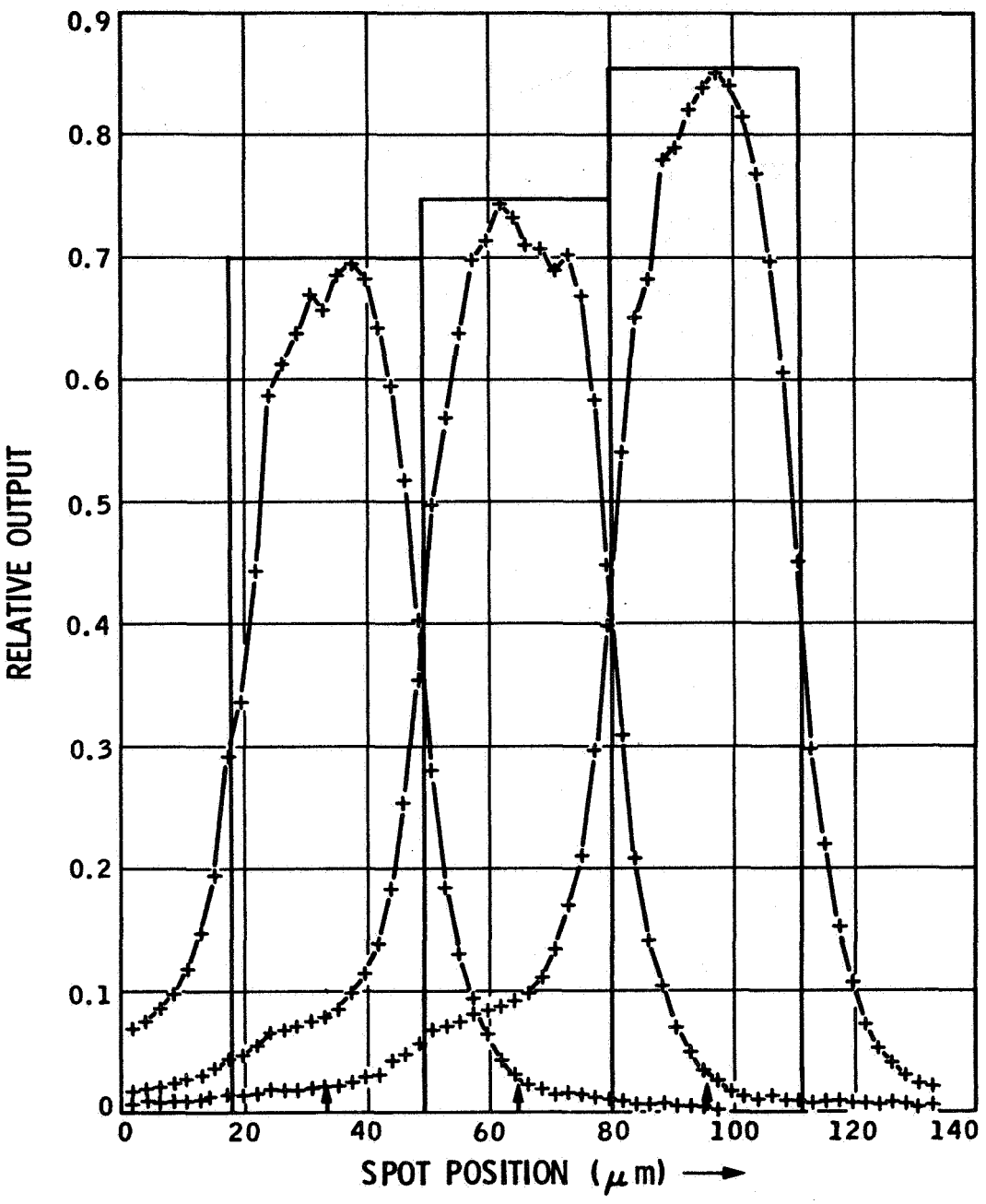

Figure 12. Sensitivity profile for three adjacent pixels (blue filter) (scan || to vertical channel)

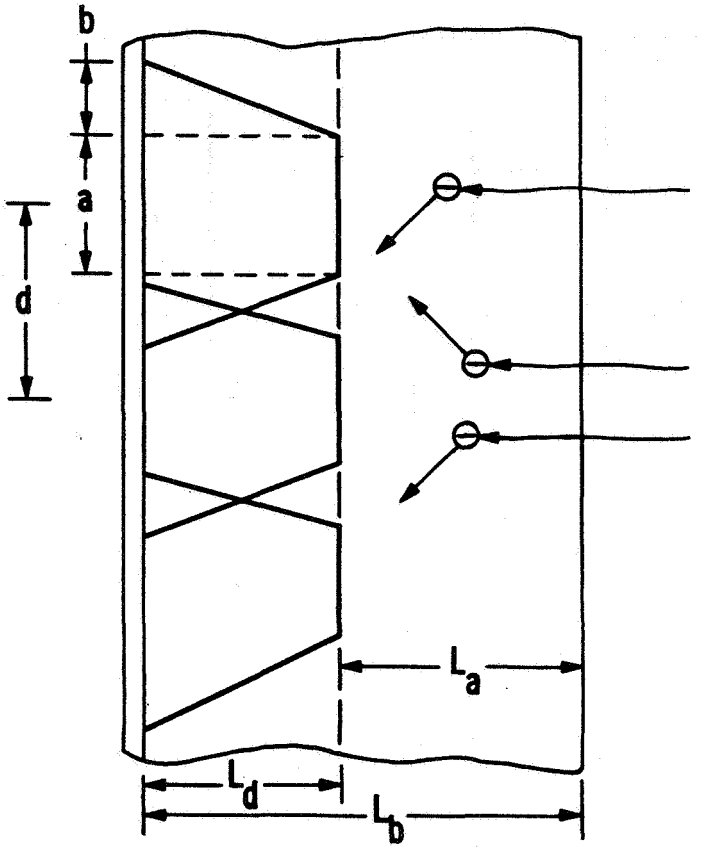

$$MTF = MTF(L.D.) \times R_T$$

$$R_T = \text{sinc}(\omega b/2)\ \text{sinc}(\omega(a+b)/2)$$

Figure 13. Schematic illustrating overlapping depletion collection profile

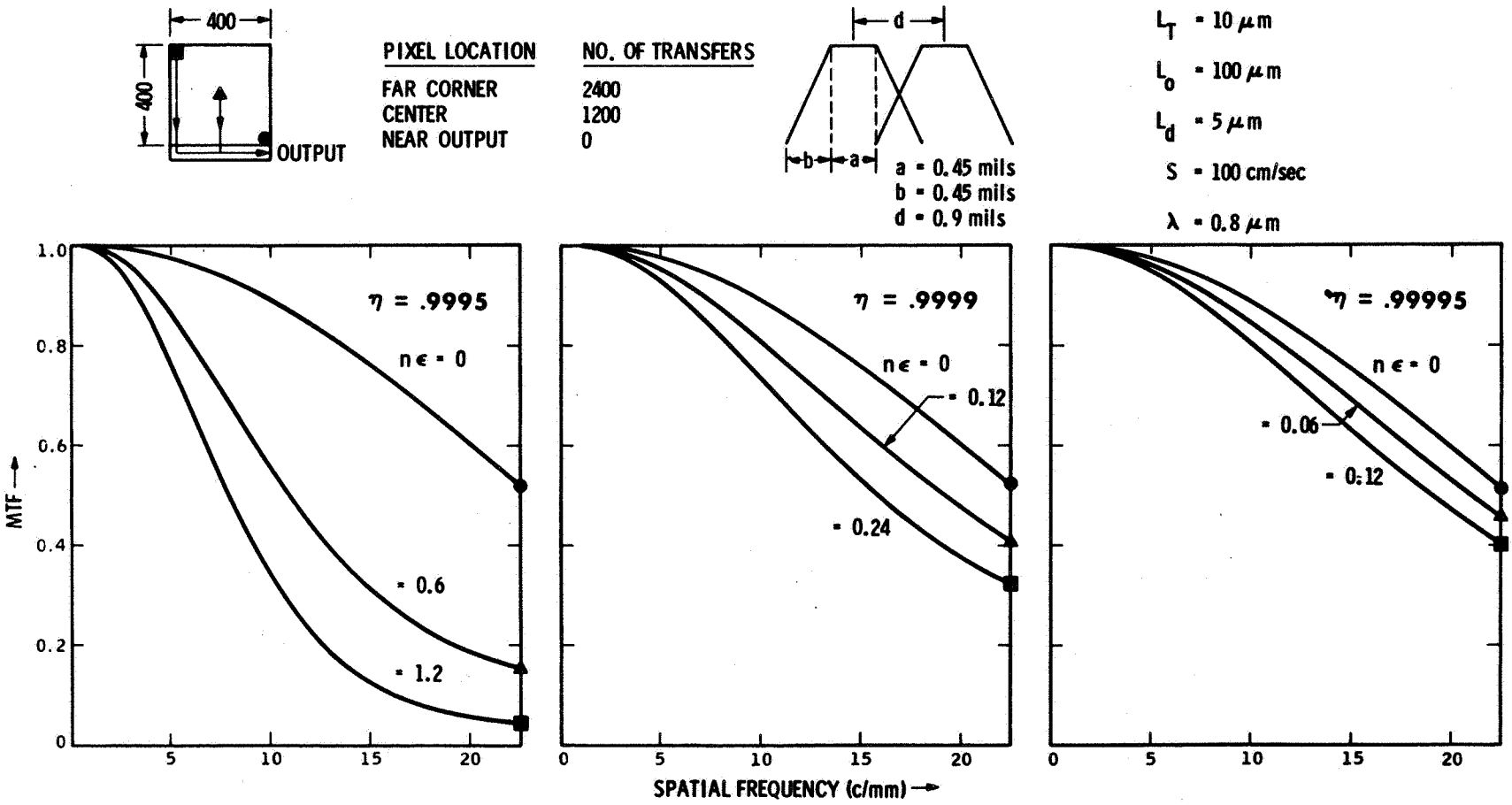

Figure 14. Calculated MTF for a 400 × 400 three-phase CCD imager (MTF = $\eta_k/\eta_0 \times$ MTF (nϵ) × R_T)

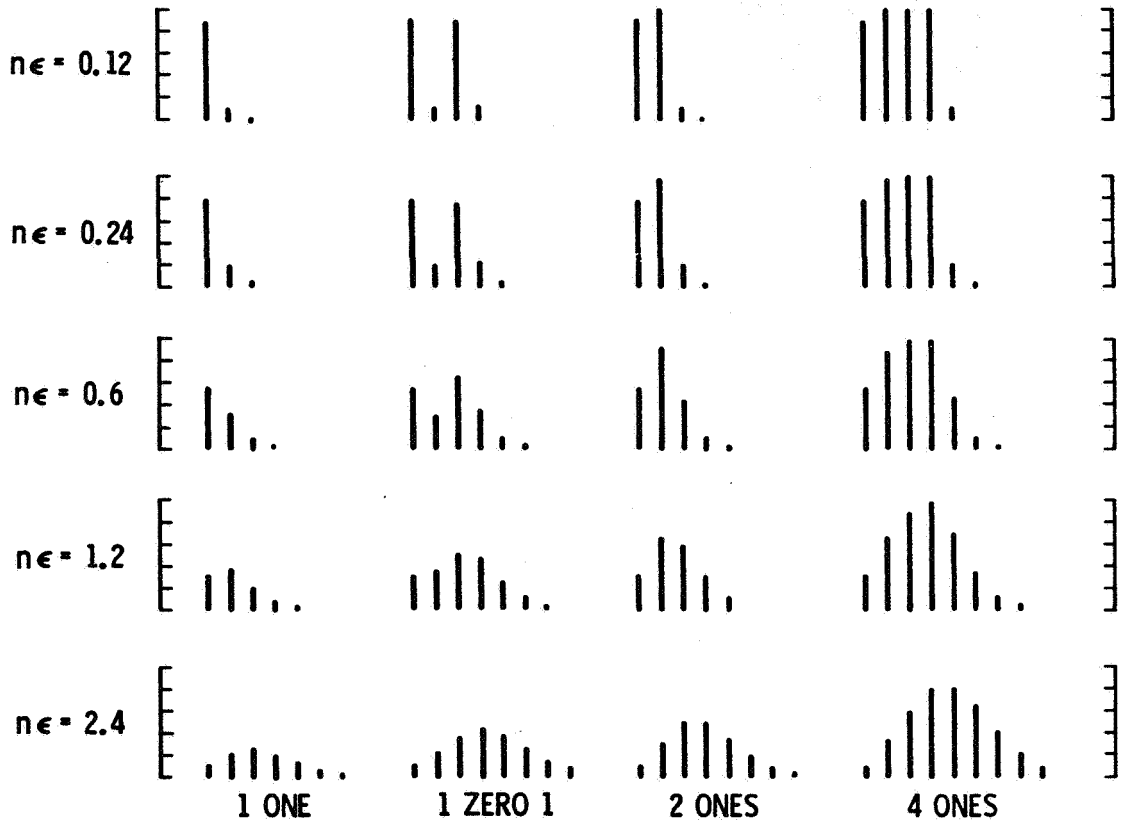

Figure 15. Charge dispersion due to transfer inefficiency (linear model $\eta + \epsilon = 1$)

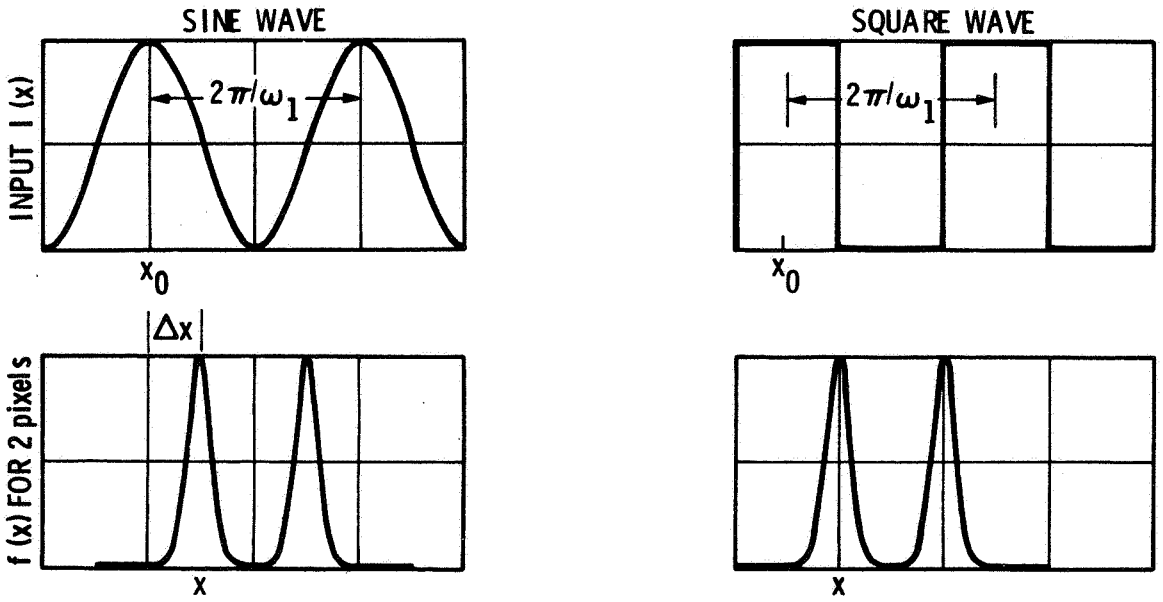

$$R(x)_{\omega=\omega_1} = \int_{-\infty}^{\infty} I(x')f(x' - x)\,dx'$$

$$= \cos \omega_1(\Delta x)F(f(x))\Big|_{\omega=\omega_1}$$

$$= \cos \omega_1(\Delta x)\,MTF(\omega_1)$$

WHERE $\Delta x = x - x_0$

$$R(x)_{\omega=\omega_1} = \int_{-\infty}^{\infty} Sq(x')f(x' - x)\,dx'$$

$$= F^{-1}\left[F(\omega)F(Sq(x))\right]$$

$$= \frac{4}{\pi} \sum_{n=1,3,5\ldots}^{\infty} (-1)^{(n-1)/2} \frac{\cos(n\omega_1\Delta x)}{n} MTF(n\omega_1)$$

Figure 16. Relation between the MTF and device response for sine- and square-wave inputs